Journal of Neuroscience Research 76:713–722 (2004)

Hyperpolarization-Activated, Cyclic Nucleotide-Gated Cation Channels: Roles in the Differential Electrophysiological Properties of Rat Primary Afferent Neurons

Huiyin Tu, Lunbin Deng, Qian Sun, Lei Yao, Ji-Sheng Han, and You Wan*
Neuroscience Research Institute, Peking University, Key Laboratory of Neuroscience (Peking University), Ministry of Education, Beijing, Peoples Republic of China

The large, medium-sized, and small neurons of the dorsal root ganglion (DRG) have different functions in the processing of various senses. Hyperpolarization-activated, cyclic nucleotide-gated channels (HCN) contribute greatly to neuronal excitability. In the present study, which used whole-cell patch clamp techniques and immunohistochemical staining methods, the electrophysiological properties of DRG neurons were systematically compared, and the roles of HCN-1, -2, and -4 were examined. The main results were as follows. 1) The large neurons had significantly higher $V_{0.5}$ values (membrane potential at which the HCN channels were half-activated) and shorter time constants (τ) than small or medium-sized DRG neurons. However, large DRG neurons had higher I_h density (HCN neuron current). 2) HCN-1 was found predominantly, but not exclusively, in large and medium-sized DRG neurons; HCN-2 was found in all DRG neurons; and HCN-4 was poorly visualized in all DRG neurons. HCN-1 and HCN-2 were colocalized in large and medium-sized neurons with immunostaining of adjacent sections. In the dorsal horn of the spinal cord, HCN-1, HCN-2, and HCN-4 were all expressed in laminae I–IV, although HCN-1 was not detectable in lamina II. 3) Blockade of I_h current in DRG neurons caused a significant decrease in $V_{0.5}$, resting membrane potential, and repetitive firing number of action potential and a significant increase in time of rising phase of action potential. These results suggest that the different HCN channels in the three types of DRG neurons might contribute to their differential electrophysiological properties.

Key words: hyperpolarization-activated, cyclic nucleotide-gated channel; I_h; dorsal root ganglion; ZD7288

The dorsal root ganglion (DRG) is the first processing station of the senses. It contains large, medium-sized, and small neurons, corresponding approximately to the Aα/Aβ-, Aδ-, and C-fibers, respectively (Brown et al., 1978; Light and Perl, 1979). The Aα/Aβ-fibers are responsible for nonpainful touch, vibration, and proprioceptive senses; the Aδ- and C-fibers are responsible for nociception. The molecular mechanisms underlying the differences among them are of great interest in developing an understanding of the process of sensation both in normal and in pathological conditions.

Hyperpolarization-activated, cyclic nucleotide-gated (HCN) channels, first identified in cardiac pacemaker cells (DiFrancesco, 1993), were also found in a variety of peripheral and central neurons (Moosmang et al., 2001; Accili et al., 2002; Robinson and Siegelbaum, 2002). These channels were slowly activated by hyperpolarization to generate depolarizing inward current (termed I_f in cardiac cells and I_h in neurons) and were permeable to both Na^+ and K^+. They play important roles in many tissues. At resting membrane potentials, about 10–15% of the HCN channels are activated and mediate about 30% of the membrane conductance. These activated HCN channels stabilize the resting membrane potential (Pape, 1996). For example, in basolateral amygdala neurons, where no I_h current was recorded, the resting membrane potential was relatively low and was near the K^+ equilibrium potential. In addition, modulation of the I_h current affects the neuronal resting membrane potential (Lamas, 1998) and excitability (Ghamari-Langroudi and Bourque, 2000). I_h contributes to the pacemaker depolarization that generates rhythmic oscillations in mammalian heart (Calabrese, 1998; Biel et al., 2002) and synaptic transmission in the brain (Beaumont and Zucker, 2000; Cuttle et al., 2001; Chevaleyre and Castillo, 2002; Mellor et al., 2002).

The first three authors contributed equally to this work.

Contract grant sponsor: National Natural Science Foundation of China; Contract grant number: 30330026; Contract grant number: 30240059; Contract grant number: 30170319; Contract grant sponsor: National Basic Research Program of China; Contract grant number: G1999054000.

*Correspondence to: You Wan, Neuroscience Research Institute, Peking University, 38 Xue Yuan Road, Beijing 100083, Peoples Republic of China. E-mail: ywan@bjmu.edu.cn

Received 8 November 2003; Accepted 28 January 2004

Published online 23 April 2004 in Wiley InterScience (www.interscience.wiley.com). DOI: 10.1002/jnr.20109

Four isoforms of HCN genes (HCN-1–4) have been cloned from mouse and human (Ludwig et al., 1998; Santoro et al., 1998). They are closely related in amino acid sequence, sharing about 60% identity, and belong to the cyclic nucleotide-gated channel superfamily (Biel et al., 2002). The expression patterns of the HCN isoforms in mammalian brain are different. HCN-2 is expressed extensively, whereas HCN-1 and HCN-4 are less numerous. The HCN isoforms also have distinct electrophysiological properties and activation kinetics, e.g., responsiveness to cAMP (Santoro and Tibbs, 1999; Ishii et al., 2001).

In DRG neurons, I_h was observed mainly in the medium-sized and large neurons (Scroggs et al., 1994). The role of HCNs in DRG neurons is of great interest. For example, HCN in DRG neurons have been found to contribute to neuropathic pain (Yao et al., 2003; Chaplan et al., 2003). In the present study, we tested the hypothesis that the expression of the various isoforms of HCN channels is the basis for the observed electrophysiological properties of DRG neurons. By using patch clamp techniques and immunohistochemical staining methods, the electrophysiological properties of the three types of DRG neurons were compared. The expression patterns of HCN isoforms 1, 2, and 4 in DRG neurons and the spinal dorsal horn were examined, and the relative contributions of HCN in different DRG neurons were investigated.

MATERIALS AND METHODS

Experimental Animals

Adult male Wistar rats (180–200 g) were used in this study. Animals were kept under a natural dark/light cycle, with unlimited access to food and water. All experiments were carried out in accordance with the National Institutes of Health *Guide for the Care and Use of Laboratory Animals* (revised in 1996) and were approved by the Animal Use and Protection Committee of our University.

Whole-Cell Patch Clamp Recording of I_h Current

DRG neurons were isolated according to the method of Study and Kral (1996). Rats were overanesthetized with sodium pentobarbital (50 mg/kg body weight, i.p.) and decapitated. DRG from lumbar segments L4 and L5 were dissected out, minced, and digested with a mixture of 0.56 mg/ml type III trypsin (Sigma, St. Louis, MO) and 1.16 mg/ml type A collagenase (Sigma) in DMEM (Gibco, Grand Island, NY) for 45 min at 37°C and agitated by gentle bubbling with 95% O_2 and 5% CO_2. Type II-S trypsin inhibitor (Sigma) was added to a final concentration of 1.44 mg/ml 10 min before the cessation of digestion. The remaining pieces of ganglion were gently triturated by using fire-polished pipettes with decreasing tip size. Dissociated cells were placed on a 35-mm plastic culture dish (Corning, Corning, NY) for 2–5 min. The bathing solution was replaced by extracellular medium before recording.

Whole-cell patch clamp recording and data acquisition were controlled by an online Apple 9600/200 MP computer programmed with HEKA Pulse V 8.03 software (HEKA Electronics). Patch pipettes (2–5 MΩ) were pulled from borosilicate glass capillaries (WPI) in a two-stage fashion on a vertical puller (model PB-7; Narishige, Tokyo, Japan) and then fire-polished in a microforge (MF-9; Narishige). Voltage clamp and current clamp were carried out by using an EPC-9 amplifier (HEKA Electronics) after a giga-ohm seal had been established. The patch electrodes were filled with intercellular solution (135 mM potassium gluconate, 2 mM $MgCl_2$, 1.1 mM EGTA, 5 mM Mg-ATP, 0.5 mM Na-GTP, and 5 mM HEPES). The pH was adjusted to 7.2 with KOH and osmolarity to 300 mOsm. The extracellular solution comprised 145 mM NaCl, 5 mM KCl, 1.5 mM $CaCl_2$, 2 mM $MgCl_2$, 6 mM D-glucose, 10 mM HEPES. The pH was adjusted to 7.4 with NaOH and osmolarity to 330 mOsm.

Patch clamp recording was similar to that described by Scroggs et al. (1994). Under voltage clamp mode, the membrane potential was clamped to −60 mV, and the I_h current was evoked by a hyperpolarizing stimulation. The current density was calculated by dividing the I_h amplitude at a test potential of −110 mV by the membrane surface area. Under current clamp mode, a series of negative or positive currents applied to the cell body was used to evoke hyperpolarization or depolarization of the membrane potential, respectively.

Data Analysis

The I_h activation curve was estimated by measuring the tail current at −110 mV after application of prepulse potentials between −60 and −130 mV. Tail currents were normalized to the maximal current (obtained at a prepulse of −110 mV). The activation curve for each neuron was fitted with a Boltzmann equation of the following form: $I_h/I_{h(max)} = 1/\{1 + exp[(V_m - V_{0.5})/k]\}$, where I_h is the peak amplitude of the tail current recorded immediately after the prepulse, $I_{h(max)}$ is the maximal current recorded after the maximal prepulse of −110 mV, V_m is the membrane potential, $V_{0.5}$ is the membrane potential at which I_h conductance is half-activated, and k is a slope factor of the curve.

The I_h curve was fitted with a single or double exponential according to the following equation: $I_t = I_{ss} + I_h \cdot \exp^{-t/\tau}$, where I_t is the current at time t, I_{ss} is the steady-state current, and τ is the time constant of I_h.

Immunohistochemical Staining of HCN-1, -2, and -4

Three deeply anesthetized rats were perfused through the aorta with 200 ml of normal saline, followed by 200 ml of 4% paraformaldehyde (PFA) in 0.1 mol/liter phosphate-buffered saline (PBS; pH 7.4). The L4 and L5 DRG and L4–L5 segments of the spinal cord were removed, postfixed in PFA, and cryoprotected overnight in 20% sucrose in 10 mM PBS. The DRG were then cut in 10-μm-thick serial sections. The spinal cord was cut in 20-μm-thick sections in a cryostat (Cryocut 1800; Leica Instruments) and mounted on gelatin/chrome alum-coated glass slides.

Immunostaining for HCN subtypes was performed as described by Ma (2002). Briefly, the cut sections were incubated overnight at 4°C in a humid chamber with one of the following primary antibodies, diluted in PBS containing 0.3% Triton X-100 and 1% bovine serum albumin: 1) 1:1,000 rabbit anti-rat HCN-1 primary antibody, 2) 1:500 rabbit anti-rat HCN-2 primary antibody, or 3) 1:200 rabbit anti-rat HCN-4 primary antibody. All antibodies were purchased from Chemicon Inter-

TABLE I. Properties of the Action Potential and the I_h Current in Three of DRG Neuron Types‡

Parameters	Small	Medium-sized	Large
Capacitance (pF)	28.6 ± 1.6 (20)	46.3 ± 3.2 (17)★	83.4 ± 5.3 (10)★
V_{rest} (mV)	−46.9 ± 1.4 (15)	−45.1 ± 0.6 (18)	−46.7 ± 1.3 (13)
V_{peak} (mV)	107.1 ± 3.4 (15)	103.6 ± 3.7 (16)	93.1 ± 3.5 (11)
$V_{threshold}$ (mV)	−12.0 ± 0.7 (15)	−14.1 ± 1.1 (16)	−26.4 ± 1.1 (11)★
$APD_{0.5}$ (ms)	2.6 ± 0.2 (15)	2.5 ± 0.2 (16)	0.9 ± 0.1 (12)★
k (mV)	11.6 ± 1.4 (14)	11.5 ± 0.6 (16)	12.6 ± 0.7 (10)
I_h density (pA/pF)	2.9 ± 0.2 (14)	5.1 ± 0.4 (16)★	10.1 ± 1.4 (10)★★†
$V_{0.5}$ (mV)	−101.9 ± 1.6 (14)	−99.5 ± 0.9 (16)	−97.3 ± 1.2 (10)★
τ (msec)	815 ± 170 (9)	646 ± 64 (14)	266 ± 17 (8)★★†
τ_{fast} (msec)	691 ± 165 (9)	285 ± 82 (14)★★	117 ± 14 (8)★★
τ_{slow} (msec)	1,735 ± 390 (9)	1,536 ± 327 (14)	907 ± 137 (8)

‡V_{rest}, resting potential; V_{peak}, peak amplitude; $V_{threshold}$, threshold potential of action potential; $APD_{0.5}$, action potential duration at half-amplitude; k, slope factor of I_h; I_h density, I_h normalized to cell capacitance; $V_{0.5}$, membrane potential at which the HCN channel was half-activated; τ, time constant determined from single exponential fits; τ_{fast}, time constant of the fast component determined from biexponential fits; τ_{slow}, time constant of the slow component determined from biexponential fits. Data are expressed as mean ± SE. The numbers in parentheses are sample size.

★$P < .05$ vs. small neurons.

★★$P < .01$ vs. small neurons.

†$P < .05$ vs. medium-sized neurons.

national (Temecula, CA). After extensive washing in 10 mM PBS, the sections were incubated with a biotinylated secondary antibody to rabbit IgG, followed by incubation with the streptavidin-conjugated horseradish peroxidase for 30 min. Sections were then washed in PBS and processed with chromogen (diaminobenzidine, 1 mg/ml; ammonium nickel sulfate, 80 mg/ml; 0.001% H_2O_2). Adjacent slides were used to detect colocalization of HCNs in DRG neurons.

Double Immunofluorescent Histochemical Staining

DRG sections were coincubated with one of the following antibody combinations: 1) rabbit anti-rat HCN-1 antibody (1:500) and goat anti-rat neurofilament 200 (NF-200; 1:4,000; Sigma), 2) rabbit anti-rat HCN-1 antibody and fluorescein isothiocyanate (FITC)-labeled isolectin B4 (IB4-FITC; 10 μg/ml; Sigma), or 3) rabbit anti-rat HCN-2 antibody (1:200) and IB4-FITC. After they were thoroughly washed, the sections were incubated in biotinylated second antibody to rabbit IgG, washed with PBS, and incubated with streptavidin-conjugated tetramethyl rhodamine isothiocyanate (TRITC; 1:1,000; Sigma) and FITC-conjugated second antibody to goat or streptavidin-conjugated TRITC for 30 min. A fluorescence microscope (DMIRB; Leica) was used to view and photograph the stained sections.

At least 500 HCN-immunoreactive neurons were measured in every animal. Neurons of different sizes were allocated to separate bins and plotted against the percentage of total neurons analyzed. To minimize statistical error, only cell bodies with a clear nucleus were used. The soma area was calculated by assuming that DRG neurons were elliptical and measuring the major and minor axes.

Statistical Analysis

Results are presented as means ± SEM. Statistical analyses were based on Friedman's nonspecific analysis of variance (ANOVA) and Fisher's exact test. Student's *t*-test was also applied where appropriate. $P < .05$ was considered significant.

RESULTS

Electrophysiological Properties of Three DRG Neuron Types

DRG neurons were classified into three types according to their diameters. In the present study, the diameters of large, medium-sized, and small neurons were 42.8 ± 0.9 μm (n = 14), 32.8 ± 0.7 μm (n = 18), and 26.4 ± 0.5 μm (n = 20), respectively. The physiological properties of the three types of DRG neurons were significantly different (Table I). The excitability was the highest and $APD_{0.5}$ (action potential duration at half amplitude) was the shortest in large neurons. The threshold of action potential ($V_{threshold}$) in large neurons was the lowest. In contrast, small DRG neurons exhibited an obvious "shoulder" during the falling phase of the action potential, resulting in longer $APD_{0.5}$ values.

I_h Current Identification

By using current-clamp recording of whole-cell patches, DRG neurons with membrane potentials lower than −45 mV were selected. The I_h current was evident as a rectifying voltage response to a step hyperpolarizing current in a time-dependent manner. Extracellular perfusion with 100 μM ZD7288 (Zeneca; molecular weight 292.81; Tocris Cookson, Inc., Ellisville, MI), a specific I_h blocker, inhibited I_h current significantly, resulting in a diminished depolarizing sag (Fig. 1A). By using voltage clamp recording, hyperpolarization stepping from −50 to −130 mV resulted in a slowly activated inward current, which was not inactivated during the course of the 1,600-msec voltage step. The current consisted of two

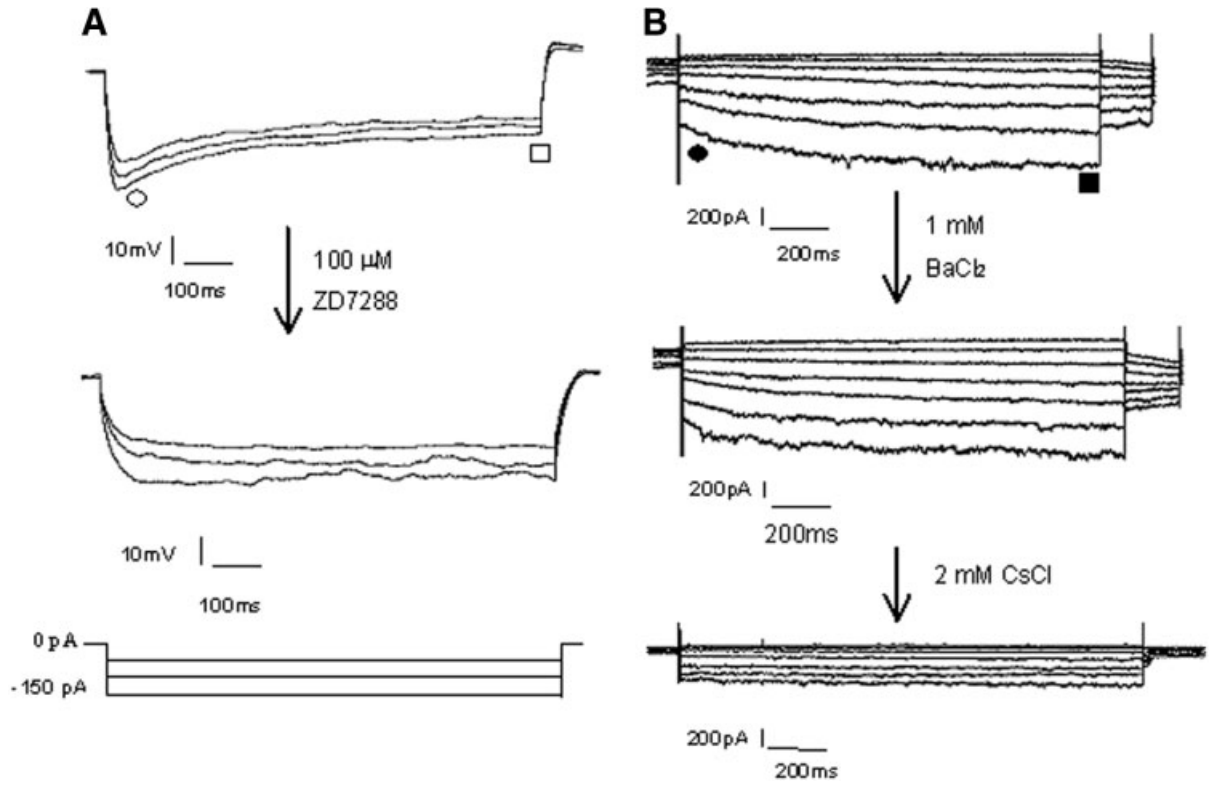

Fig. 1. I_h current identification. I_h was sensitive to blockade by extracellular perfusion with 100 μM ZD7288 (**A**) and 2 mmol/liter CsCl, but not 1 mmol/liter $BaCl_2$ (**B**). Note that, in A, two types of voltage evoked by injection of a series of negative current pluses (approximately –50 to –150 pA, 1,000 msec, –50 pA in step) were recorded under current clamp mode: instantaneous voltage (open circle) and stead-state current (open square). As a result, a voltage-dependent, depolarizing "sag" in the membrane potential occurred, indicating the activation of I_h. In B, two types of current evoked by membrane hyperpolarization were recorded under voltage clamp mode: instantaneous current (solid circle) and stead-state current (solid square).

distinct components: an instantaneous inward current (I_{ins}) and a slowly activated steady-state current (I_{ss}; Fig. 1B). I_h was measured by subtraction of I_{ins} from I_{ss}. I_h was found to be sensitive to extracellular Cs^+, but not Ba^{2+}, a typical characteristic of I_h currents described previously (Scroggs et al., 1994; Wang et al., 1997). At a test potential of −110 mV, I_h current was almost completely inhibited in the presence of 2 mM Cs^+ (average blockade 88.4% ± 2.4%; n = 5). In contrast, extracellular application of 1 mM Ba^{2+} did not significantly reduce I_h amplitude (average blockade 11.4% ± 1.1%; n = 7).

I_h Current Distribution Pattern in DRG Neurons

I_h was recorded in 23% (18/78) of small, 79% (27/34) of medium-sized, and 100% (14/14) of large neurons. The incidence of I_h in large and medium-sized neurons was significantly higher than that in small neurons ($P < .001$). The amplitude and density of I_h in large and medium-sized neurons were also much higher than those in small neurons. The peak I_h amplitude measured at a test potential of –110 mV was 1,112.2 ± 151.8 pA, 324.0 ± 33.6 pA, and 70.9 ± 5.1 pA in large, medium-sized, and small neurons, respectively (Fig. 2A). To determine whether the observed differences in amplitude were caused by the differences in cell surface area, the I_h current density (pA/pF, normalized to cell capacitance) was calculated. We found significant differences in I_h current density among the three types of DRG neurons (Table I). The I_h current density in large, medium-sized, and small DRG neurons was 10.1 ± 1.4, 5.1 ± 0.4, and 2.9 ± 0.2 pA/pF (normalized to cell capacitance), respectively ($P < .05$).

I_h Activation Curves in DRG Neurons

From the activation curves (Fig. 2B), the value of $V_{0.5}$ in large DRG neurons (–97.3 ± 1.2, n = 10) was significantly higher than that in small DRG neurons (–101.9 ±, 1.6; n = 14; $P < .05$). The slope factors (k) for large, medium-sized, and small neurons (12.6 ± 0.7, 11.5 ± 0.6, and 11.6 ± 1.4 mV, respectively) were not significantly different ($P > .05$; Table I). The time constant in the large and medium-sized neurons was 266 ± 17 and 646 ± 64 msec, respectively, which was significantly shorter than that in small neurons (815 ± 170 msec; $P < .05$).

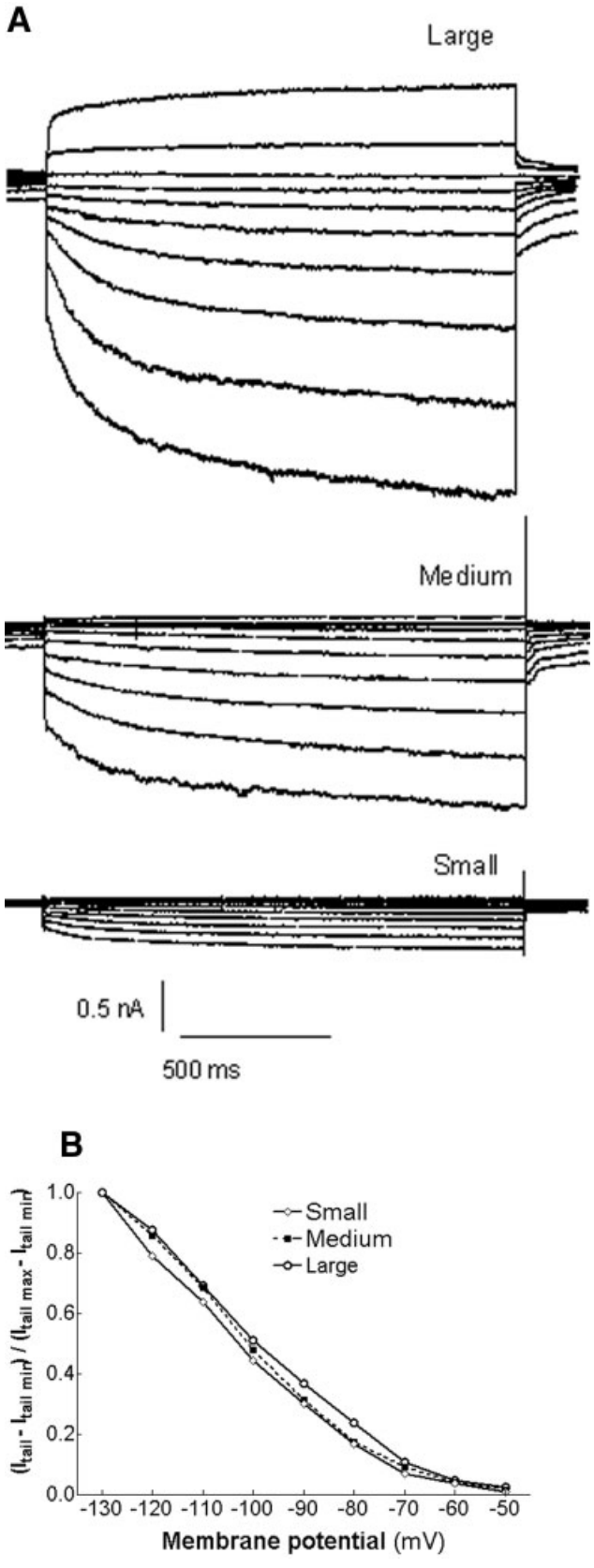

Expression of HCNs in DRG

Immunohistochemical results revealed a subgroup of elliptical or elongated neurons in DRG stained with antibodies specific to HCN-1, -2, or -4 (Fig. 3A1–3). The HCN immunoreactivity was more concentrated in the plasma membrane, HCN-1 being expressed more prominently than other HCN isoforms. Over 40% of the DRG neurons were HCN-1 positive. Most of them were medium-sized to large neurons (soma area $>800\ \mu m^2$). In contrast, HCN-2 was expressed in all DRG neurons but at a lower level (Fig. 3C). In some small neurons, HCN-2 was prominently stained. Very interestingly, no HCN-4 expression was detected in any of the DRG neurons.

The intensity of HCN immunoreactivity in individual DRG neurons varied substantially. The highest intensity was observed in large DRG neurons (soma area around $1{,}800\ \mu m^2$ or more), which account for approximately 10% of the total neurons. Most medium-sized neurons (cell body area 1,000 to $1{,}800\ \mu m^2$) were moderately stained. On adjacent 10-μm sections, immunohistochemical staining revealed that HCN-1 and HCN-2 seemed to colocalize on the membranes of large and medium-sized DRG neurons, and also to small regions of small neurons (Fig. 3B1,2).

Double Immunofluorescent Histochemical Staining of HCN

HCN-1 and NF-200 were stained in large and medium-sized DRG neurons (Fig. 4A1–3). HCN-1 was not doubly stained with IB4 (Fig. 4B1–3). In contrast, HCN-2 was doubly stained with IB4 in small DRG neurons (Fig. 4C1–3). These results confirm that HCN-1 was present mainly in large DRG neurons (Fig. 4A1), and HCN-2 was found in all neurons (Fig. 4C1).

Expression of HCNs in the Spinal Dorsal Horn

In the dorsal horn of the spinal cord, the positive HCN-1 immunoreactivities were found mainly in lamina I and III–IV; there was no staining in lamina II. Both HCN-2 and HCN-4 were labeled in all layers of the spinal dorsal horn (Fig. 5). In addition, dense immunostaining of HCN-1, -2, and -4 was observed in the large motor neurons in the ventral horn of the spinal cord.

Fig. 2. I_h activation curves in the three DRG neuron types. The activation curve of I_h was estimated by measuring the tail current (I_{tail}) at −120 mV after application of prepulse potentials between −60 and −130 mV. Tail currents were normalized to the maximal current (obtained at a prepulse of −110 mV). The activation curve for each neuron was fitted with a Boltzmann equation of the following forms: $I_h/I_{h(max)} = (I_{tail} - I_{tail(min)}/I_{tail(max)} - I_{tail(min)}) = 1/\{1 + exp[V_m - V_{0.5}]/k\}$, where I_h is the peak amplitude of the tail current recorded immediately after the prepulse, $I_{h(max)}$ is the maximum current recorded after the maximal prepulse of −110 mV, V_m is the membrane potential, $V_{0.5}$ is the membrane potential at which I_h conductance is half-activated, and k is a slope factor of the curve.

Effect of ZD7288, an I_h-Specific Blocker, on the Electrophysiological Properties of DRG Neurons

To activate the I_h current, serial hyperpolarizing stimuli of −60 mV to −130 mV for 1,600 msec were applied to DRG neurons when the membrane potential was clamped to −60 mV. Boltzmann fitting showed that the $V_{0.5}$ and the slope factor (k) were −100.2 ± 0.5 mV and 9.4 ± 0.4 mV, respectively. Fifteen minutes after the addition of 50 μM ZD7288, the activation curve of I_h current moved toward the hyperpolarizing direction (Fig. 6) and $V_{0.5}$ was hyperpolarized significantly to −105.1 ± 0.3 mV (n = 4; $P < .001$), whereas k was unchanged (9.0 ± 1.2 mV; n = 4). In addition, ZD7288 increased the time constant (τ) as the values of τ decreased when the membrane potential was hyperpolarized. After perfusion with ZD7288, the activation curve shifted significantly to the hyperpolarization direction.

After application of ZD7288 for 15 min, the resting membrane potential (V_{rest}) was decreased significantly from −52.0 ± 1.1 mV to −58.3 ± 1.1 mV (n = 7; $P < .01$). A series of hyperpolarizing current stimuli (from 0 to 400 pA, step at 40 pA, duration of 5 msec) was applied to induce a burst of action potentials. ZD7288 blockade increased the duration of the rising phase of the action potentials in DRG neurons. It was found that the action potential rising time increased from 6.3 ± 0.4 msec to 7.1 ± 0.5 msec after application of 50 μM ZD7288 for 15 min (n = 7; $P < .01$). Other parameters of the action potential, such as peak amplitude (V_{peak}), posthyperpolarization amplitude (V_{AHP}), duration at half-amplitude ($APD_{0.5}$), threshold ($V_{threshold}$), and time of falling phase, did not change significantly (Table II).

In addition, ZD7288 decreased the number of repetitive firings of DRG neurons. A threshold stimulus of 500-msec duration could induce repetitive firing in parts of neurons. After application of ZD7288, the interspike interval of the repetitive action potential increased and the number of action potentials decreased from 7.0 ± 1.1 to 4.7 ± 0.7 (n = 3; $P < .05$; Table II).

Action Potential Profiles in Small DRG Neurons With or Without I_h

All small neurons were classified into two groups according to whether the I_h current was present. Neurons with the I_h current possessed a noninflected action potential profile and had shorter action potential durations. Neurons without an I_h current possessed an inflected action potential profile and had longer action potential durations. The action potential duration at half-amplitude ($APD_{0.5}$) was 2.3 ± 0.2 and 4.3 ± 0.7 for neurons with and without I_h current, respectively (n = 7; $P < .05$).

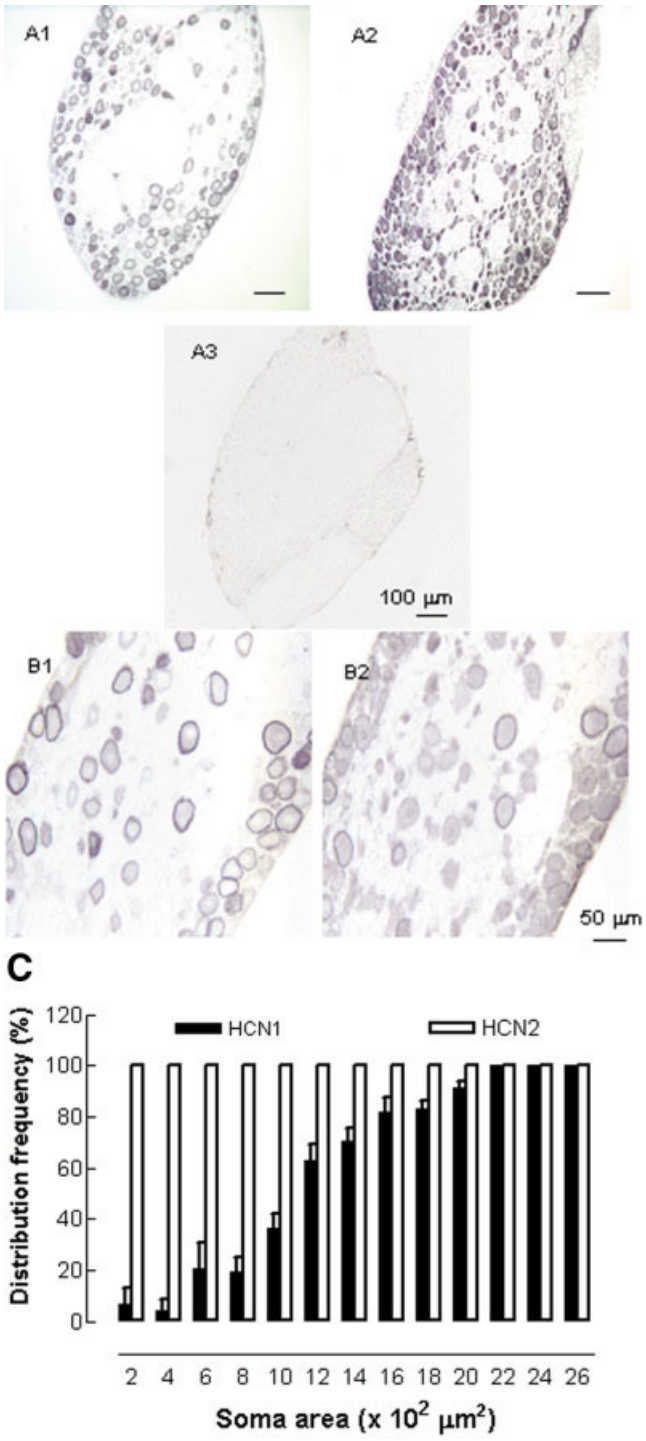

Fig. 3. Immunohistochemical staining of HCNs: colocalization and frequency distribution in three DRG neuron types. **A:** Immunohistochemical staining of HCN-1, -2, and -4 in DRG. **A1:** HCN-1; **A2:** HCN-2; **A3:** HCN-4. HCN-1 was labeled in large and medium-sized neurons and concentrated in the plasma membrane; HCN-2 was labeled in all DRG neurons; HCN-4 was not detected in DRG neurons. B: Colocalization of HCN-1 and HCN-2 in large and medium-sized DRG neurons on adjacent slides. **B1:** HCN-1; **B2:** HCN-2. **C:** Frequency distribution of HCN-1 and HCN-2 in rat DRG neurons of different size. HCN-1 was distributed mainly in large and medium-sized DRG neurons. HCN-2 was distributed in all types of DRG neurons. Figure can be viewed in color online via www.interscience.wiley.com.

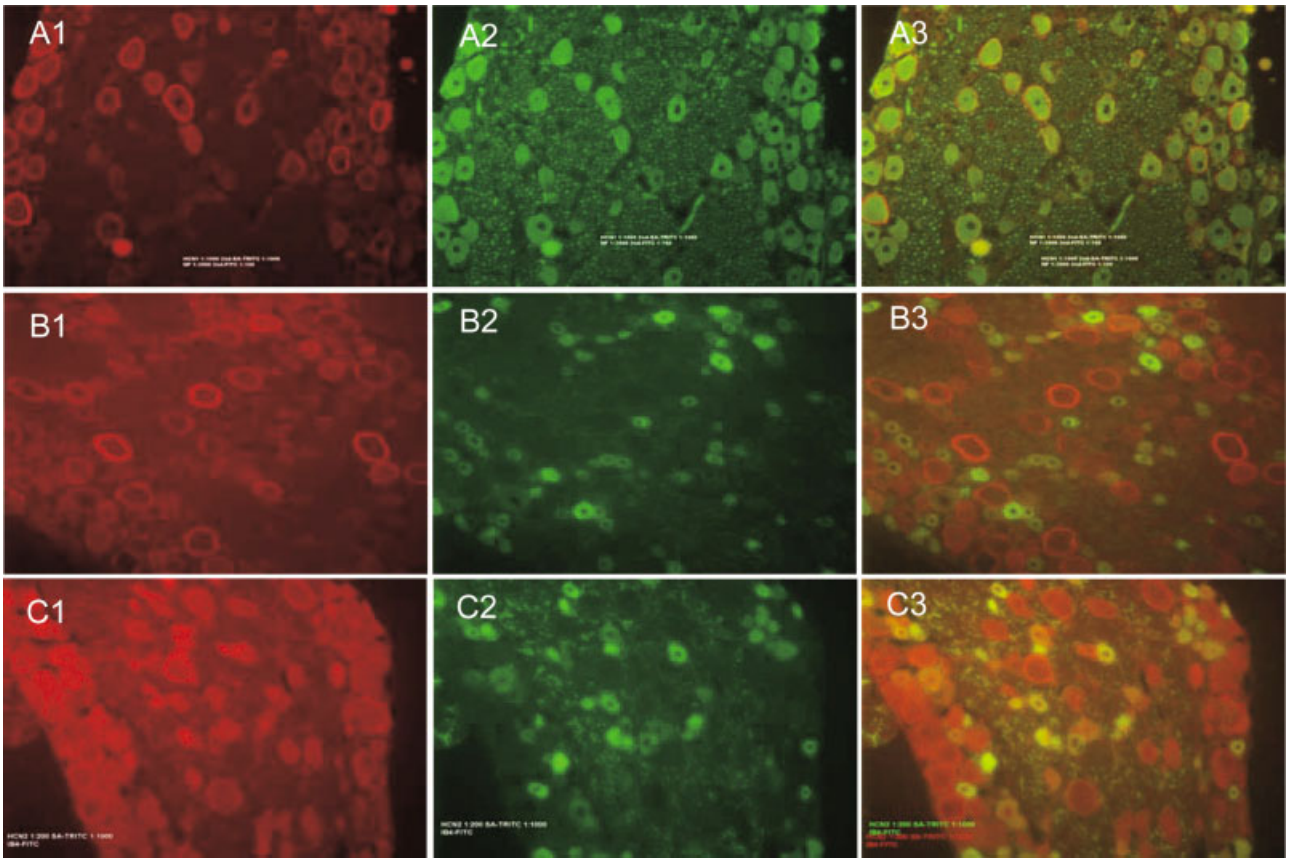

Fig. 4. Double staining of HCN-1 or -2 with neuronal markers. **A1:** HCN-1; **A2:** NF200 (a myelinated fiber marker); **A3:** HCN-1 + NF200. HCN-1 was doubly stained with NF200. **B1:** HCN-1; **B2:** FITC-labeled isolectin B4 (IB4-FITC); **B3:** HCN-1 + IB4-FITC. HCN-1 was not doubly stained with IB4. **C1:** HCN-2; **C2:** IB4-FITC; **C3:** HCN-2 + IB4-FITC. HCN-2 was doubly stained with IB4.

There was no significant difference in other parameters of the action potential in these two groups of neurons.

DISCUSSION

In the present study combining electrophysiological and immunohistochemical methods, we observed the differential electrophysiological properties of the three types of DRG neurons and the distribution pattern of HCN-1, -2, and -4 isoforms in DRG neurons and the spinal dorsal horn. DRG neurons were characterized as three subtypes based on their average diameter: large ($d \geq 40$ μm), medium-sized (40 μm $> d \geq 30$ μm), and small ($d < 30$ μm). The grouping criteria correspond approximately to the categories of Aα/Aβ-, Aδ-, and C-fibers, respectively (Study and Kral, 1996). It is well known that the large, myelinated Aα/Aβ fibers are responsible for non-painful light touch, vibration, and proprioceptive senses; the medium, myelinated Aδ fibers or small, unmyelinated C fibers are responsible for nociception.

As shown in Table I, the three types of DRG neurons had different electrophysiological properties. Large neurons had much lower threshold potentials ($V_{threshold}$) and shorter action potential durations (APD) than the small and medium-sized neurons, although their resting membrane potentials were similar.

Many molecular mechanisms, especially differences in the ion channel composition and distribution, underlie the observed electrophysiological properties of different DRG neurons. The present study emphasizes the importance of HCN in these phenomena. First, the distribution pattern, current density, and I_h activation curves were all different in the three types of DRG neurons. The I_h current was recorded in a cell type-specific manner in DRG neurons and was found in 23% of the small, 79% of medium-sized, and 100% of the large neurons (Fig. 3C). The I_h density was also significantly greater in the large cells than in the medium-sized or small cells. This difference was not solely a reflection of the variation in surface area (Fig. 3C). In addition, from the activation curves of the three types of DRG neurons (Fig. 2), $V_{0.5}$ in the large neurons was much higher than that in the medium-sized and small neurons, indicating that the I_h current in the large neurons was more easily activated. This speculation is also supported by the results of the immuno-

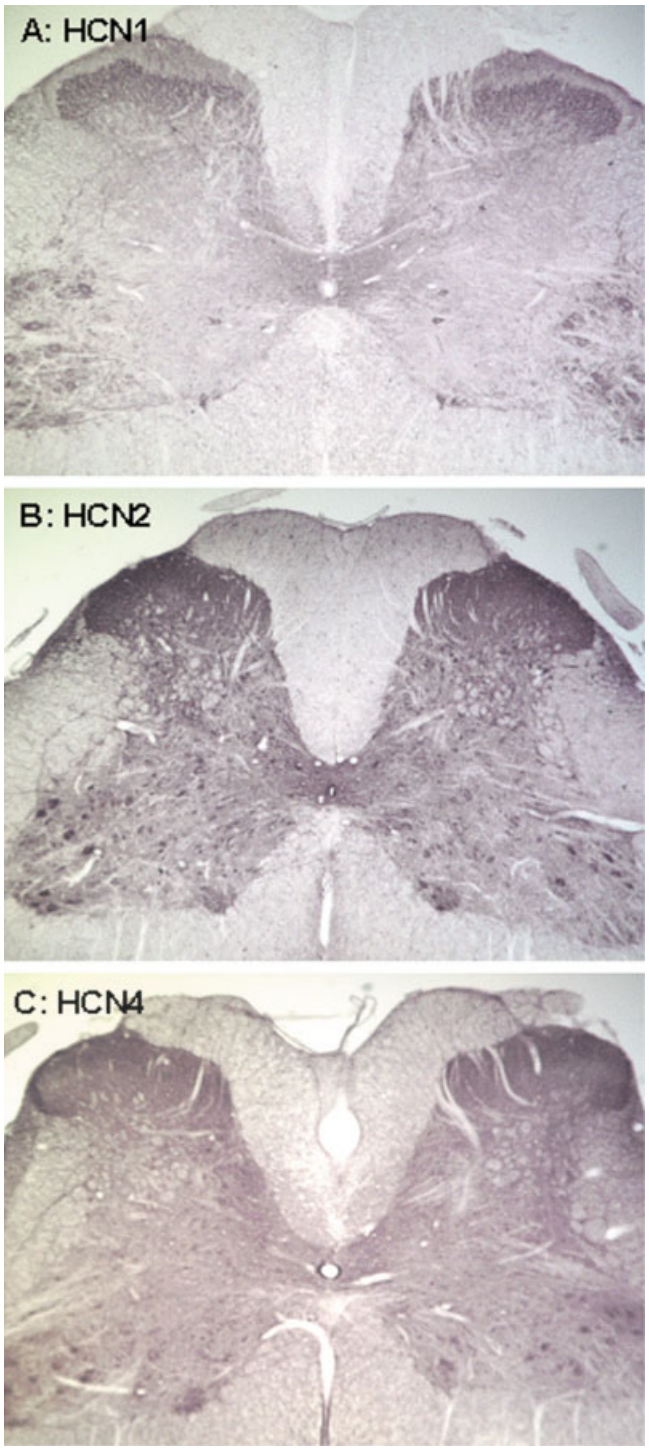

Fig. 5. Immunohistochemical localization of HCN-1, -2, and -4 in the spinal dorsal horn. HCN-1 was detected in lamina I, III, and IV but absent in lamina II (**A**); HCN-2 (**B**) and HCN-4 (**C**) were detected in lamina I–IV. Figure can be viewed in color online via www.interscience.wiley.com.

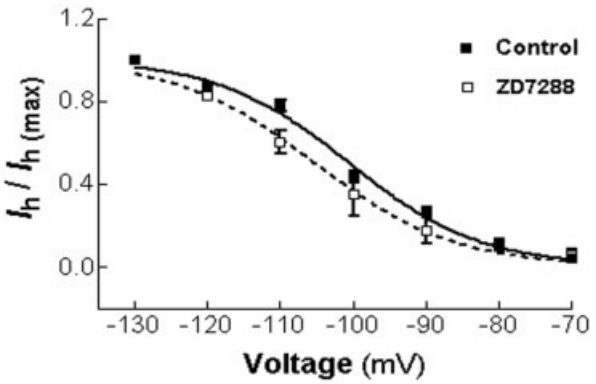

Fig. 6. Blockade of I_h induced a small, but significant, leftward shift of the I_h activation curve as revealed by Boltzmann regression analysis.

TABLE II. Effects of I_h Blockade With a Specific I_h Blocker (ZD7288) on Action Potential Parameters and I_h Current in DRG Neurons†

Parameters	Control	ZD7288
V_{rest} (mV)	−52.0 ± 1.1 (7)	−58.3 ± 1.1 (7)**
V_{peak} (mV)	104.1 ± 3.0 (7)	97.5 ± 6.7 (7)
$V_{threshold}$ (mV)	−16.8 ± 1.4 (7)	−17.6 ± 1.1 (7)
VA_{HP} (mV)	14.4 ± 2.2 (7)	15.1 ± 2.2 (7)
$AP_{rising\ time}$ (msec)	6.3 ± 0.4 (7)	7.1 ± 0.5 (7)**
$AP_{falling\ time}$ (msec)	4.0 ± 0.8 (7)	4.4 ± 0.8 (7)
$APD_{0.5}$ (msec)	2.0 ± 0.5 (7)	2.2 ± 0.7 (7)
Repetitive firing number	7.0 ± 1.1 (3)	4.7 ± 0.3 (3)**
$V_{0.5}$ (mV)	−100.2 ± 0.5 (4)	−105.1 ± 0.3 (4)**
k (Slope factor of I_h)	9.4 ± 0.4 (4)	9.0 ± 1.2 (4)

†V_{peak}, peak amplitude; $V_{threshold}$, action potential threshold; V_{AHP}, after-hyperpolarization amplitude; AP, action potential; $AP_{rising\ time}$, action potential rising time; $AP_{falling\ time}$, action potential falling time; $APD_{0.5}$, action potential duration at half-amplitude; $V_{0.5}$, membrane potential at which the HCN channel was half-activated; *k* slope factor of I_h. Data are expressed as mean ± SE. The numbers in parentheses are sample size.
**$P < .01$ vs. corresponding control.

histochemical staining, with which the highest intensity signals were detected in large DRG neurons (Figs. 3, 4). These data are consistent with other findings (Pearce and Duchen, 1994; Scroggs et al., 1994).

The HCN-1, -2, and -4 isoforms are expressed differently in the various DRG neurons. HCN-1 was found predominantly, but not exclusively, in large and medium-sized DRG neurons, and this was confirmed by the colabeling of HCN-1 with NF-200, a marker of myelinated fibers (Fig. 4). HCN-2 was detected in all DRG neurons, confirming previous reports that this channel is distributed in the primary sensory neurons (Moosmang et al., 2001). HCN-4 was poorly visualized in all the DRG neurons. HCN-3 was not examined because of the lack of a commercially available antibody.

Blockade of I_h affected the electrophysiological properties of DRG neurons. ZD7288 [4-(N-ethyl-N-phenylamino)-1,2-dimethyl-6-(methylamino)pyridinium

chloride] was developed as a bradycardiac in the 1990s. It blocks I_h (or funny current, I_f, in cardiac Purkinje cells). It is also a specific I_h blocker in neurons (Harris and Constanti, 1995; Satoh and Yamada, 2000; Seutin et al., 2001). Perfusion with 50 μM ZD7288 for 15 min significantly decreased the resting membrane potential (V_{rest}) and increased the action potential rising time ($AP_{rising\ time}$). It also caused a significant decrease in the repetitive firing number and the $V_{0.5}$ (the membrane potential at which HCN channel was half-activated; Table II). These results indicate that the activated HCN channels might help to stabilize the resting membrane potential in the resting state and drive the membrane potential depolarization to the threshold of action potential, elevating neuronal excitability. The effects of ZD7288 blockade were confirmed by the differences observed in small DRG neurons with or without I_h current: a noninflected action potential in neurons with I_h current and an inflected action potential in neurons without I_h current. That is, the duration of their action potentials was different.

The distribution pattern of HCNs in DRG neurons and the spinal dorsal horn might have important consequences. First, it may constitute the molecular basis underlying the different functions of DRG neurons of different sizes. Second, different HCNs in medium-sized, myelinated Aδ fibers or small, unmyelinated C fibers might be related to nociception. Chaplan et al. (2003) and Yao et al. (2003) reported that HCN in DRG neurons were important in nociception. Third, HCN-1 and -2 might play roles in processing the other senses, especially touch under normal conditions, as HCN-1 and -2 colocalized in large, myelinated Aα- and Aβ-fibers. In addition, under chronic pain conditions, HCN-1 and -2 in Aα- and Aβ-fibers might have functions in allodynia or hyperalgesia.

The I_h current is activated when the membrane potential is hyperpolarized. It can also be regulated by intracellular cAMP. The slowly activating hyperpolarization-activated inward current recorded in the present study shares many properties with the I_h current observed in central and peripheral neurons. For example, hyperpolarizing pulses from −60 to −130 mV triggered this slowly activated, inward current. DRG cell bodies exhibited a depolarizing "sag" in response to negative current injection. After addition of cAMP to the perfusion of DRG neurons, the activation curve was shifted to the right (data not shown). The current was almost completely blocked by extracellular 2 mM Cs^+ but not by 1 mM Ba^{2+}. Extracellular perfusion with 50 μM ZD7288, a specific blocker of I_h, efficiently abolished this effect, suggesting that activation of I_h was responsible for time-dependent rectification (Fig. 1). An inward rectifier current (I_{IR}) is another hyperpolarization-activated inward rectifier found in DRG neurons (Scroggs et al., 1994). However, I_{IR} was activated more rapidly and was blocked by both Ba^{2+} and Cs^+. These distinct electrophysiological properties enabled us to distinguish I_h from I_{IR}.

The study of I_h in DRG neurons is confounded by contradictory findings. Doan and Kunze (1999) recorded I_h current in all A- and C-type neurons, but other workers could not record I_h current in small DRG neurons (Tokimasa and Akasu, 1990; Ingram and Williams, 1996) or only in subgroups (~30–40%) of small DRG neurons (Scroggs et al., 1994; Yagi and Sumino, 1998). This inconsistency might be due to the presence of different isoforms of HCN or the different activation kinetics of HCN isoforms in DRG neurons (Santoro and Tibbs, 1999; Ishii et al., 2001; Kaupp and Seifert, 2001). In the present study, HCN-2 was immunohistochemically stained in all small DRG neurons, although I_h current was recorded in a subpopulation of them (data not shown).

Another interesting phenomenon was the colocalization of different HCN isoforms in DRG neurons. HCN-1 and HCN-2 were coexpressed in large and medium-sized neurons (Fig. 3B1,2). HCN proteins form hetero- or homopolymers (Ulens and Tytgat, 2001). Wild-type HCN channels may form heteromeric complexes with non-HCN accessory proteins (Chen et al., 2001). It is possible that the coexpressed HCN-1 and HCN-2 might also form complexes. The formation of polymers will greatly influence HCN function. For example, in hypothalamic neurons possessing HCN-2 channels only, the I_h current could not be recorded. However, in hypothalamic neurons possessing both HCN-1 and HCN-2 channels, the I_h current was obvious (Santoro et al., 2000). Although these channels are closely related in amino acid sequence, their electrophysiological properties and activation kinetics are distinct. For example, the time constants for activation follow the series: HCN-1 < HCN-2 < HCN-3 < HCN-4. In addition, HCN-1 has the lowest sensitivity to cAMP (Ludwig et al., 1998, 1999; Santoro et al., 1998; Santoro and Tibbs, 1999; Ishii et al., 2001; Biel et al., 2002). The I_h current is activated with a faster time constant and a larger magnitude in A-type neurons (Doan and Kunze, 1999). In DRG neurons, there also may exist hetero- or homopolymers of HCN. The presence of HCN polymers in DRG neurons of different sizes might be one of the mechanisms underlying their different electrophysiological properties and I_h characteristics.

The central termination of primary afferent neurons in the spinal cord dorsal horn is topographically organized. Large-caliber, myelinated Aα- and Aβ-fibers terminate in laminae III–IV (Light and Perl, 1979); small-caliber, myelinated Aδ-fibers terminate in lamina I, and small, unmyelinated C-fibers terminate in lamina II (Rethelyi, 1977; Brown et al., 1978; Light and Perl, 1979). According to this distribution pattern, it is not surprising that HCN-1 and HCN-2 were expressed in all layers of the spinal cord dorsal horn, whereas HCN-1 was not detectable in layer II (Fig. 5). The presence of HCN-4 in all layers of the dorsal horn is surprising, insofar as it is not expressed in any type of DRG neuron. The simplest explanation for this is that cells (neurons and glial cells) in the dorsal horn express HCN-4 or that the descending fibers synthesize HCN protein. We found HCN-4 immunostaining in isolated neurons from the superficial layers of the spinal dorsal horn, confirming this speculation (data not shown). In addition, HCN-1, -2, and -4 were all densely stained in motor neurons of the ventral horn in the spinal

cord. It was reasonable to speculate that HCNs might play a role in movement regulation.

In summary, the cell type-specific expression pattern of HCN isoforms and current properties of I_h current in primary afferent neurons strongly suggest that HCNs have functional significance in the processing of different senses under physiological and pathological conditions and possibly also in the regulation of movement.

ACKNOWLEDGMENT

The authors thank Dr. Richard A. Collins (Hong Kong DNA Chips Ltd.) for help in preparing the manuscript.

REFERENCES

Accili EA, Proenza C, Baruscotti M, DiFrancesco D. 2002. From funny current to HCN channels: 20 years of excitation. News Physiol Sci 17:32–37.

Beaumont V, Zucker RS. 2000. Enhancement of synaptic transmission by cyclic AMP modulation of presynaptic I_h channels. Nat Neurosci 3:133–141.

Biel M, Schneider A, Wahl C. 2002. Cardiac HCN Channels. Structure, function, and modulation. Trends Cardiovasc Med 12:206.

Brown AG, Rose PK, Snow PJ. 1978. Morphology and organization of axon collaterals from afferent fibres of slowly adapting type I units in cat spinal cord. J Physiol 277:15–27.

Calabrese RL. 1998. Cellular, synaptic, network, and modulatory mechanisms involved in rhythm generation. Curr Opin Neurobiol 8:710–717.

Chaplan SR, Guo H-Q, Lee D, Luo H, Liu C, Kuei C, Velumian AA, Butler MP, Brown SM, Dubin AE. 2003. Neuronal hyperpolarization-activated pacemaker channels drive neuropathic pain. J Neurosci 23: 1169–1178.

Chen S, Wang J, Siegelbaum SA. 2001. Properties of hyperpolarization-activated pacemaker current defined by coassembly of HCN1 and HCN2 subunits and basal modulation by cyclic nucleotide. J Gen Physiol 117:491–504.

Chevaleyre V, Castillo PE. 2002. Assessing the role of I_h channels in synaptic transmission and mossy fiber LTP. Proc Natl Acad Sci USA 99:9538–9543.

Cuttle MF, Rusznak Z, Wong AY, Owens S, Forsythe ID. 2001. Modulation of a presynaptic hyperpolarization-activated cationic current (I(h)) at an excitatory synaptic terminal in the rat auditory brainstem. J Physiol 534:733–744.

DiFrancesco D. 1993. Pacemaker mechanisms in cardiac tissue. Annu Rev Physiol 55:455–472.

Doan TN, Kunze DL. 1999. Contribution of the hyperpolarization-activated current to the resting membrane potential of rat nodose sensory neurons. J Physiol 514:125–138.

Ghamari-Langroudi M, Bourque CW. 2000. Excitatory role of the hyperpolarization-activated inward current in phasic and tonic firing of rat supraoptic neurons. J Neurosci 20:4855–4863.

Harris NC, Constanti A. 1995. Mechanism of block by ZD 7288 of the hyperpolarization-activated inward rectifying current in guinea pig substantia nigra neurons in vitro. J Neurophysiol 74:2366–2378.

Ingram SL, Williams JT. 1996. Modulation of the hyperpolarization-activated current (I_h) by cyclic nucleotides in guinea-pig primary afferent neurons. J Physiol 492:97–106.

Ishii TM, Takano M, Ohmori H. 2001. Determinants of activation kinetics in mammalian hyperpolarization-activated cation channels. J Physiol 537:93–100.

Kaupp UB, Seifert R. 2001. Molecular diversity of pacemaker ion channels. Annu Rev Physiol 63:235–257.

Lamas JA. 1998. A hyperpolarization-activated cation current (I_h) contributes to resting membrane potential in rat superior cervical sympathetic neurones. Pflugers Arch 436:429–435.

Light AR, Perl ER. 1979. Spinal termination of functionally identified primary afferent neurons with slowly conducting myelinated fibers. J Comp Neurol 186:133–150.

Ludwig A, Zong X, Jeglitsch M, Hofmann F, Biel M. 1998. A family of hyperpolarization-activated mammalian cation channels. Nature 393: 587–591.

Ludwig A, Zong X, Stieber J, Hullin R, Hofmann F, Biel M. 1999. Two pacemaker channels from human heart with profoundly different activation kinetics. EMBO J 18:2323–2329.

Ma QP. 2002. Expression of capsaicin receptor (VR1) by myelinated primary afferent neurons in rats. Neurosci Lett 319:87–90.

Mellor J, Nicoll RA, Schmitz D. 2002. Mediation of hippocampal mossy fiber long-term potentiation by presynaptic I_h channels. Science 295:143–147.

Moosmang S, Stieber J, Zong X, Biel M, Hofmann F, Ludwig A. 2001. Cellular expression and functional characterization of four hyperpolarization-activated pacemaker channels in cardiac and neuronal tissues. Eur J Biochem 268:1646–1652.

Pape HC. 1996. Queer current and pacemaker: the hyperpolarization-activated cation current in neurons. Annu Rev Physiol 58:299–327.

Pearce RJ, Duchen MR. 1994. Differential expression of membrane currents in dissociated mouse primary sensory neurons. Neuroscience 63: 1041–1056.

Rethelyi M. 1977. Preterminal and terminal axon arborizations in the substantia gelatinosa of cat's spinal cord. J Comp Neurol 172:511–528.

Robinson RB, Siegelbaum SA. 2003. Hyperpolarization-activated cation currents: from molecules to physiological function. Annu Rev Physiol 65:453–480.

Santoro B, Tibbs GR. 1999. The HCN gene family: molecular basis of the hyperpolarization-activated pacemaker channels. Ann N Y Acad Sci 868:741–764.

Santoro B, Liu DT, Yao H, Bartsch D, Kandel ER, Siegelbaum SA, Tibbs GR. 1998. Identification of a gene encoding a hyperpolarization-activated pacemaker channel of brain. Cell 93:717–729.

Santoro B, Chen S, Luthi A, Pavlidis P, Shumyatsky GP, Tibbs GR, Siegelbaum SA. 2000. Molecular and functional heterogeneity of hyperpolarization-activated pacemaker channels in the mouse CNS. J Neurosci 20:5264–5275.

Satoh TO, Yamada M. 2000. A bradycardiac agent ZD7288 blocks the hyperpolarization-activated current (I(h)) in retinal rod photoreceptors. Neuropharmacology 39:1284–1291.

Scroggs RS, Todorovic SM, Anderson EG, Fox AP. 1994. Variation in IH, IIR, and ILEAK between acutely isolated adult rat dorsal root ganglion neurons of different size. J Neurophysiol 71:271–279.

Seutin V, Massotte L, Renette MF, Dresse A. 2001. Evidence for a modulatory role of I_h on the firing of a subgroup of midbrain dopamine neurons. Neuroreport 12:255–258.

Study RE, Kral MG. 1996. Spontaneous action potential activity in isolated dorsal root ganglion neurons from rats with a painful neuropathy. Pain 65:235–242.

Tokimasa T, Akasu T. 1990. Cyclic AMP regulates an inward rectifying sodium-potassium current in dissociated bull-frog sympathetic neurones. J Physiol 420:409–429.

Ulens C, Tytgat J. 2001. Gi- and Gs-coupled receptors up-regulate the cAMP cascade to modulate HCN2, but not HCN1 pacemaker channels. Pflugers Arch 442:928–942.

Wang Z, Van Den Berg RJ, Ypey DL. 1997. Hyperpolarization-activated currents in the growth cone and soma of neonatal rat dorsal root ganglion neurons in culture. J Neurophysiol 78:177–186.

Yagi J, Sumino R. 1998. Inhibition of a hyperpolarization-activated current by clonidine in rat dorsal root ganglion neurons. J Neurophysiol 80:1094–1104.

Yao H, Donnelly DF, Ma C, LaMotte RH. 2003. Upregulation of the hyperpolarization-activated cation current after chronic compression of the dorsal root ganglion. J Neurosci 23:2069–2074.